Critical process parameters of gelatin microparticle fabrication with a water-in-oil emulsion method

Burak Demir, Michael C. Hacker

Suggested Citation:
Demir, B., & Hacker, M. (2025). Critical process parameters of gelatin microparticle fabrication with a water-in-oil emulsion method. International Journal of Pharmaceutics, 686, Article 126302. https://doi.org/10.1016/j.ijpharm.2025.126302

International Journal of Pharmaceutics 686 (2025) 126302

Contents lists available at ScienceDirect

International Journal of Pharmaceutics

journal homepage: www.elsevier.com/locate/ijpharm

Critical process parameters of gelatin microparticle fabrication with a water-in-oil emulsion method

Burak Demir, Michael C. Hacker *

Heinrich Heine University Duesseldorf, Faculty of Mathematics and Natural Sciences, Institute of Pharmaceutics and Biopharmaceutics Universitaetsstrasse 1, 40225 Duesseldorf, Germany

ARTICLE INFO

Keywords:
Protein microspheres
Water-in-oil emulsion method
Design of experiments
Particle size distribution
Particle shape parameters

ABSTRACT

Gelatin-based microparticles have received growing attention as versatile biomaterials over the years. In this study, we investigated the fabrication process of gelatin microparticles with an emulsifier-free water-in-oil technique using design of experiments (DoE). We executed three DoEs for two different gelatin types (type A and type B). We demonstrated that stirring speed is the most significant factor affecting shape parameters of sphericity of particles derived from both gelatin types. An effect of process temperature was only significant for gelatin type A particles. Water-to-oil phase volume ratio was only investigated for type B gelatin and found to impact particle sphericity of microparticles. We also showed a correlation between particle size distribution and shape factors, where an inferior particle shape quality was associated with finer particles. Through 21 verification batches at constant factor settings, we demonstrated high process performance for microparticles (gelatin type B). Overall, we demonstrated effective control in particle size distribution and particle shape factors for both gelatin types. The fabricated gelatin microparticles will subsequently be chemically crosslinked and the achieved control of particle sphericity will be beneficial for the quality of the crosslinked particles.

1. Introduction

For years, gelatin-based microparticles have attracted growing interest as a versatile biomaterial, demonstrating potential as enzymatically degradable particulate templates for the assembly of microtissues formed by adhesive cells (Hinkelmann et al., 2022a; Hinkelmann et al., 2022b; Lu et al., 2016; Nii, 2021; Pearce et al., 2021; Sakai et al., 2011; Yan et al., 2016), as well as for the delivery of therapeutic proteins and drugs (Cao et al., 2021; Curcio et al., 2010; Gunji et al., 2013; Hinkelmann et al., 2022a; Hinkelmann et al., 2022b; Patel et al., 2008; Turner et al., 2017; Vandelli et al., 2001; Wang et al., 2000; Yang et al., 2020). Due to the aqueous solubility and poor thermal stability of gelatin, gelatin microparticles need to be crosslinked prior to their use in any of the aforementioned applications (Foox and Zilberman, 2015). In literature, several fabrication methods have been reported that describe the fabrication of crosslinked gelatin microparticles. Those can be classified as water-in-oil (W/O) (Hinkelmann et al., 2022b; Loth et al., 2014; Lu et al., 2016; Patel et al., 2008; Peng et al., 2011) and water-in-water (W/W) emulsion techniques (Kong et al., 2011), microfluidic fabrication (Jung and Oh, 2014; Park et al., 2016; Yeh et al., 2013), and spray drying (Bruschi et al., 2003; Tran et al., 2013). While microfluidic methods may yield monodisperse particles, their throughput and scalability are limited, and they are often constrained by the complexity and limitations of chip design (Yue et al., 2025). Spray drying method enables high-throughput fabrication but poses challenges in controlling particle size and morphology, and is associated with high operational costs (Behrend-Keim et al., 2023; Yue et al., 2025). Emulsion techniques on the other hand are particularly desirable due to their relatively low cost and ease of process handling (Yue et al., 2025).

Our group has been using a two-step fabrication method based on a W/O emulsion technique to fabricate oligomer-crosslinked gelatin microparticles (cGM). The first step involves the fabrication of GM, followed by second step, where post-fabrication covalent crosslinking is carried out using anhydride-containing oligomers of various chemical compositions (Hinkelmann et al., 2022a; Hinkelmann et al., 2022b; Loth et al., 2014). The two-step method enables control over mass input and particle quality (size distribution and shape) during post-fabrication crosslinking. This approach allows separate control of particle formation and crosslinking, enabling precise adjustment of crosslinking reaction conditions without affecting the initial morphology. In comparison to in-situ crosslinking methods, this approach allows flexible control over crosslinking density, as crosslinker amount, base type/

* Corresponding author.
E-mail addresses: burak.demir@hhu.de (B. Demir), michael.hacker@hhu.de (M.C. Hacker).

https://doi.org/10.1016/j.ijpharm.2025.126302
Received 22 August 2025; Received in revised form 20 October 2025; Accepted 21 October 2025
Available online 25 October 2025

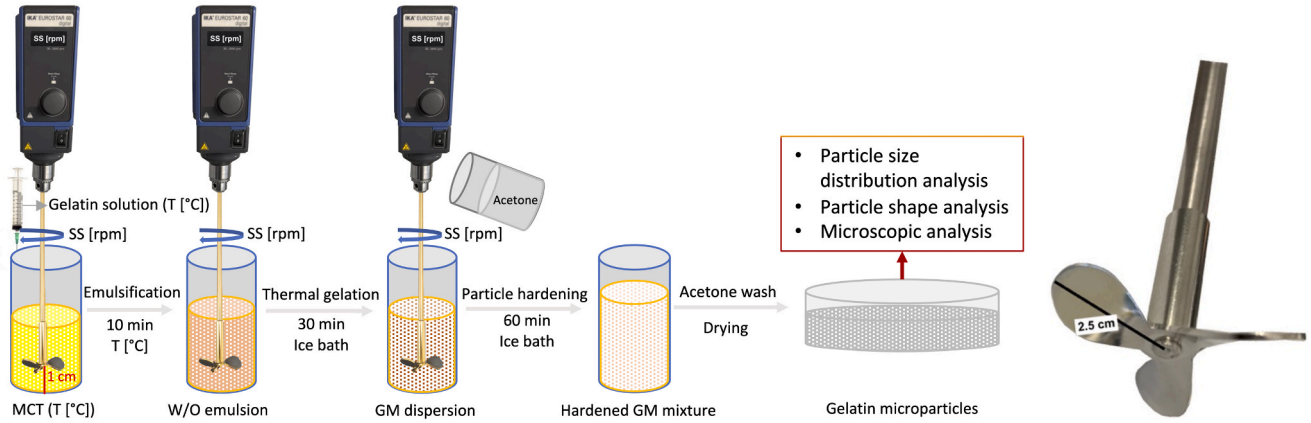

Fig. 1. Illustration of fabrication set-up, fabrication process and characterization methods. Fabrication set-up consists of an overhead stirrer with a three-bladed propeller-type stirrer (right) and a 400 ml beaker. The propeller stirrer was positioned 1 cm above the bottom of the beaker. During the emulsification stage, temperature was controlled using a heating plate equipped with temperature sensor while for thermal gelation and acetone hardening steps, cooling was performed using ice bath. GM: gelatin microparticles, MCT: medium-chain triglycerides, SS: stirring speed, T: temperature.

amount, and reaction conditions can be adjusted in predefined ranges (Loth et al., 2014).

Since the properties of crosslinked gelatin microparticles are strongly dependent on the morphology of the pristine templates, achieving reproducible particle size and shape during fabrication represents a critical step in the overall process. For application in microtissue assembly (Hinkelmann et al., 2022a; Hinkelmann et al., 2022b), spherical particles are prerequisite to facilitate correlations of particle properties and composition with biological effects, including biomaterial mineralization, cell adhesion, cell proliferation and differentiation. Controlling particle size and shape revealed challenging using the W/O emulsion technique that we utilize without an emulsifying agent or additional kinetic stabilization. Nevertheless, the absence of an emulsifier was a key factor in order to ensure that the particle surface consists of only gelatin and crosslinking oligomers.

To fabricate gelatin-based microparticles, this sequence of operations – fabrication of pristine microparticles, subsequent crosslinking to stabilize the polymer network, and finally drug loading – is essential for achieving reproducible and predictable material performance. In microtissue engineering, shape and size distribution strongly influence cell attachment and aggregate formation (D'Angelo et al., 2011; Hinkelmann et al., 2022a). Conversely, the crosslinking density of the microparticles significantly alters swelling and degradation characteristics, which in turn determine drug release profiles (Choy et al., 2008; Nguyen et al., 2015; Nouri-Felekori et al., 2019; Wang et al., 2000). Moreover, rational material design should also take into account potential electrostatic interactions between gelatin and the drug, which vary with gelatin type and can further affect drug release (Annamalai et al., 2018; Obata et al., 2012; Patel et al., 2008; Turner et al., 2017). Therefore, the stepwise approach – starting with GM fabrication process understanding, followed by crosslinking process optimization and drug loading – aligns with Quality by Design (QbD) principles and provides control over each stage according to the desired final material properties, quality and drug release profiles.

In order to identify critical process parameters that influence particle size distribution and particle shape, we employed three statistical experimental designs (DoE) to investigate the pristine GM fabrication process for two gelatin types – one obtained in an acidic process (type A) and one product of a basic process (type B). Although parameters such as gelatin solution concentration, oil type, stirrer type/geometry, and particle drying method can also be critical for the fabrication process, this study focused on three key factors: stirring speed, emulsification temperature, and water-to-oil phase volume ratio. While many studies on emulsion-based microparticle preparation have been reported, there is a lack of DoE-based investigations addressing the influence of gelatin type and processing conditions on particle morphology. The present work aims to provide a systematic understanding of how these parameters govern particle formation and morphology for different gelatin types. Therefore, it represents the first stage of a stepwise development approach, providing insights that can be translated to subsequent crosslinking and drug loading steps within the framework of QbD principles.

2. Materials and methods

2.1. Materials

Gelatin type A (~300 g Bloom) and type B (~225 g Bloom) were purchased from Merck KGaA (Darmstadt, Germany). Medium-chain triglycerides (MYRITOL® 318, now: Kollisolv®, MCT 70) was purchased from Caesar & Loretz GmbH (Hilden, Germany). Acetone and isopropanol were used in technical grade. Demineralized water was obtained by Barnstead™ MicroPure™ water purification system (Thermo Fisher Scientific GmbH, Dreieich, Germany).

2.2. Fabrication of gelatin microparticles

GM were fabricated using emulsifier-free W/O emulsion method, implemented from previously published methods (Hinkelmann et al., 2022a; Hinkelmann et al., 2022b; Loth et al., 2014). The fabrication procedure consists of three-stages: emulsification, thermal gelation and particle dehydration /hardening in acetone. The fabrication set-up consists of a 400 ml glass beaker, an overhead stirrer (Eurostar 60 control, IKA-Werke GmbH & Co. KG, Staufen, Germany) equipped with a three-bladed propeller-type tool (Fig. 1). Initially, 5 g of gelatin (either from type A ~ 300 g Bloom or type B ~ 225 g Bloom) was dissolved in 50 ml of demineralized water at pre-selected temperature. In parallel, 200 ml of medium-chain triglycerides were heated to the same temperature in the fabrication set-up and stirred at pre-defined speeds [rpm]. When the desired process temperature was reached, the gelatin solution (either 25 ml or 50 ml, depending on the phase volume ratio (R)) was added to the oil phase using a 21 G canula and the resultant mixture was emulsified for 10 min. In the second stage, the heating element was changed to an ice-bath and thermal gelation of emulsion droplets was induced by continued stirring for 30 min. Finally, 100 ml of chilled (in ice-bath) technical-grade acetone was added to the dispersion and stirred for an additional 60 min to complete particle dehydration and hardening. Finally, GM were recovered from the mixture by filtration and washed while still wet using approximately 25 ml of fresh acetone 5 times. The resultant GM were dried under the fume hood for

Table 1
List of experimental runs and conditions. DoE runs were based on the rotatable Circumscribed Central Composite Design (CCC) with alpha values of 1.414, and 1.682 for the two-factor DoEs and the three-factor DoE, respectively. All DoE runs were executed in a randomized order. Verification batches (n = 21) were fabricated to check the performance and reproducibility of the process for type B GM.

Gelatin type	Experiment type	Experimental run	Stirring speed [rpm]	Temperature [°C]	Water-to-oil phase volume ratio
Type B	Preliminary-1	P1	500	40.0	0.250
Type B	Preliminary-2	P2	500	70.0	0.250
Type B	Preliminary-3	P3	800	50.0	0.250
Type B	Preliminary-4	P4	1000	60.0	0.250
Type B	DoE-1	N1	700	50.0	0.125
Type B	DoE-1	N2	900	50.0	0.125
Type B	DoE-1	N3	700	70.0	0.125
Type B	DoE-1	N4	900	70.0	0.125
Type B	DoE-1	N5	700	50.0	0.250
Type B	DoE-1	N6	900	50.0	0.250
Type B	DoE-1	N7	700	70.0	0.250
Type B	DoE-1	N8	900	70.0	0.250
Type B	DoE-1	N9	632	60.0	0.188
Type B	DoE-1	N10	968	60.0	0.188
Type B	DoE-1	N11	800	43.0	0.188
Type B	DoE-1	N12	800	77.0	0.188
Type B	DoE-1	N13	800	60.0	0.082
Type B	DoE-1	N14	800	60.0	0.293
Type B	DoE-1	N15	800	60.0	0.188
Type B	DoE-1	N16	800	60.0	0.188
Type B	DoE-1	N17	800	60.0	0.188
Type B	DoE-2	N1	700	50.0	0.250
Type B	DoE-2	N2	900	50.0	0.250
Type B	DoE-2	N3	700	70.0	0.250
Type B	DoE-2	N4	900	70.0	0.250
Type B	DoE-2	N5	659	60.0	0.250
Type B	DoE-2	N6	941	60.0	0.250
Type B	DoE-2	N7	800	46.0	0.250
Type B	DoE-2	N8	800	74.0	0.250
Type B	DoE-2	N9	800	60.0	0.250
Type B	DoE-2	N10	800	60.0	0.250
Type B	DoE-2	N11	800	60.0	0.250
Type B	Verification batches	V1-V21	700	50.0	0.125
Type A	Preliminary-5	P5	500	60.0	0.250
Type A	Preliminary-6	P6	1000	60.0	0.250
Type A	DoE-3	N1	700	50.0	0.250
Type A	DoE-3	N2	900	50.0	0.250
Type A	DoE-3	N3	700	70.0	0.250
Type A	DoE-3	N4	900	70.0	0.250
Type A	DoE-3	N5	659	60.0	0.250
Type A	DoE-3	N6	941	60.0	0.250
Type A	DoE-3	N7	800	46.0	0.250
Type A	DoE-3	N8	800	74.0	0.250
Type A	DoE-3	N9	800	60.0	0.250
Type A	DoE-3	N10	800	60.0	0.250
Type A	DoE-3	N11	800	60.0	0.250

two days and vacuum dried (vacuum dehydration at a minimum of 10 mbar pressure) at room temperature for an additional day.

2.3. Design of experiments

Circumscribed central composite design (CCC) was used to create response-surface models for executed DoEs as the process was presumed to also yield non-linear factor response relationships. Design rotatability was assured by positioning the star points (α = 1.414 for two-factor design, and α = 1.682 for three-factor design). Several preliminary batches of GM were fabricated before executing DoE runs to gain initial process information (Table 1). The experimental runs for each DoE set were randomized to avoid systematic errors. The results were analyzed and plotted using MODDE 13 Pro (Version number: 13.0, Sartorius AG, Goettingen, Germany). Models were fitted using multiple linear regression (MLR) method. In the case of skewed response distribution, the necessary response transformations were applied using appropriate functions to normalize the response distribution and improve the prediction power of a model. Significant effects were determined using ANOVA test at a confidence level of 95 %. The visualization of further data was performed using Origin Pro (Version number: 2024b, Originlab Corporation, Massachusetts, USA).

2.4. Particle characterization

Particle size distribution of fabricated GM batches was characterized using laser diffraction (Mastersizer 3000 equipped with Hydro SV dispersion unit, Malvern Panalytical GmbH, Kassel, Germany). For diffraction measurements, particle dispersion in isopropanol (1 mg/ml) was introduced to HydroSV dispersion unit that was filled with isopropanol and stirred at 1200 rpm. Triplicate measurements for each batch were performed by maintaining laser obscuration range between 5–7 %, and the results were expressed as a volume distribution using Fraunhofer approximation. The de Brouckere mean diameter (D[4,3]) and interquartile range (IQR) were used as descriptive responses for GM size distribution.

Particle shape characterization was performed by light microscopy equipped with a camera (Leica DMLB, Leica Microsystems GmbH, Wetzlar, Germany) and dynamic image analysis (DIA) (Sync Analyzer, Microtrac Retsch GmbH, Haan, Germany). For DIA measurements, 250 mg of particles were introduced into the TurboSnyc Unit that was previously set to 0.5 psi dispersion pressure, and the particle pictures were recorded. Particle shape characterization was performed based on two shape parameters; sphericity (SPH) and length-to-width aspect ratio (AR) according to ISO 9276-6:2008 (Standardization, 2008) (Eqs. (1) and (2)). Although there is no established consensus on a specific SPH threshold, values greater than 0.95 should indicate highly spherical particles. The AR on the other hand is a well-studied shape parameter in pharmaceutical pellet manufacturing, and pellets exhibiting an AR ≤ 1.1 were assigned a good shape quality (Kleinebudde, 1995). In this study, batch percentage of the fraction of particles with SPH values higher than 0.95 (SPH ≥ 0.95) or with AR lower than 1.1 (AR ≤ 1.1) were considered as spherical particles and yields within these fractions were used as shape descriptive responses in the DoE.

$$SPH = \frac{Area\ \ equivalent\ \ diameter\ \ (Da)}{Perimeter\ \ equivalent\ \ diameter\ \ (Dp)} \quad (1)$$

$$L \Big/ W\ Aspect\ Ratio = \frac{FLength}{FWidth} \quad (2)$$

where the letter “F” represents Feret calculations.

3. Results and discussion

Fig. 2 illustrates exemplary GM from measurements of the DoE with high/low SPH and AR values. AR is the overall shape parameter whereas SPH is also affected by the surface roughness. It was noticeable in the examples that SPH values were lower, or/and AR values were higher once particle shape deviated from being spherical or particle aggregates were analyzed.

Cumulative particle size distribution plots for each DoE and verification batches for gelatin type B microparticles (GM type B) were shown in Fig. 3. In general, under the same fabrication settings, GM type A were larger than GM type B. This is likely due to the viscosity difference of

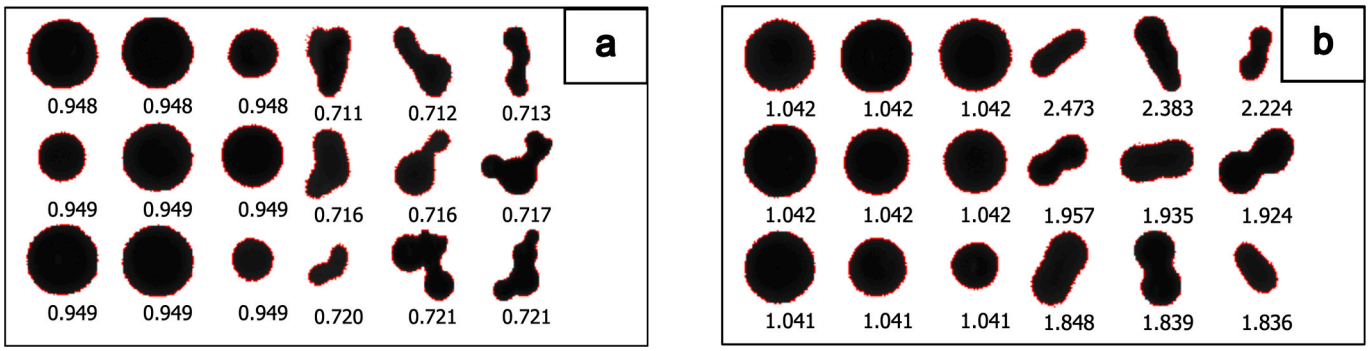

Fig. 2. Illustration for GM shapes as visualized by dynamic image analysis (DIA): a) Exemplary particles with high/low SPH values and b) with high/low AR values.

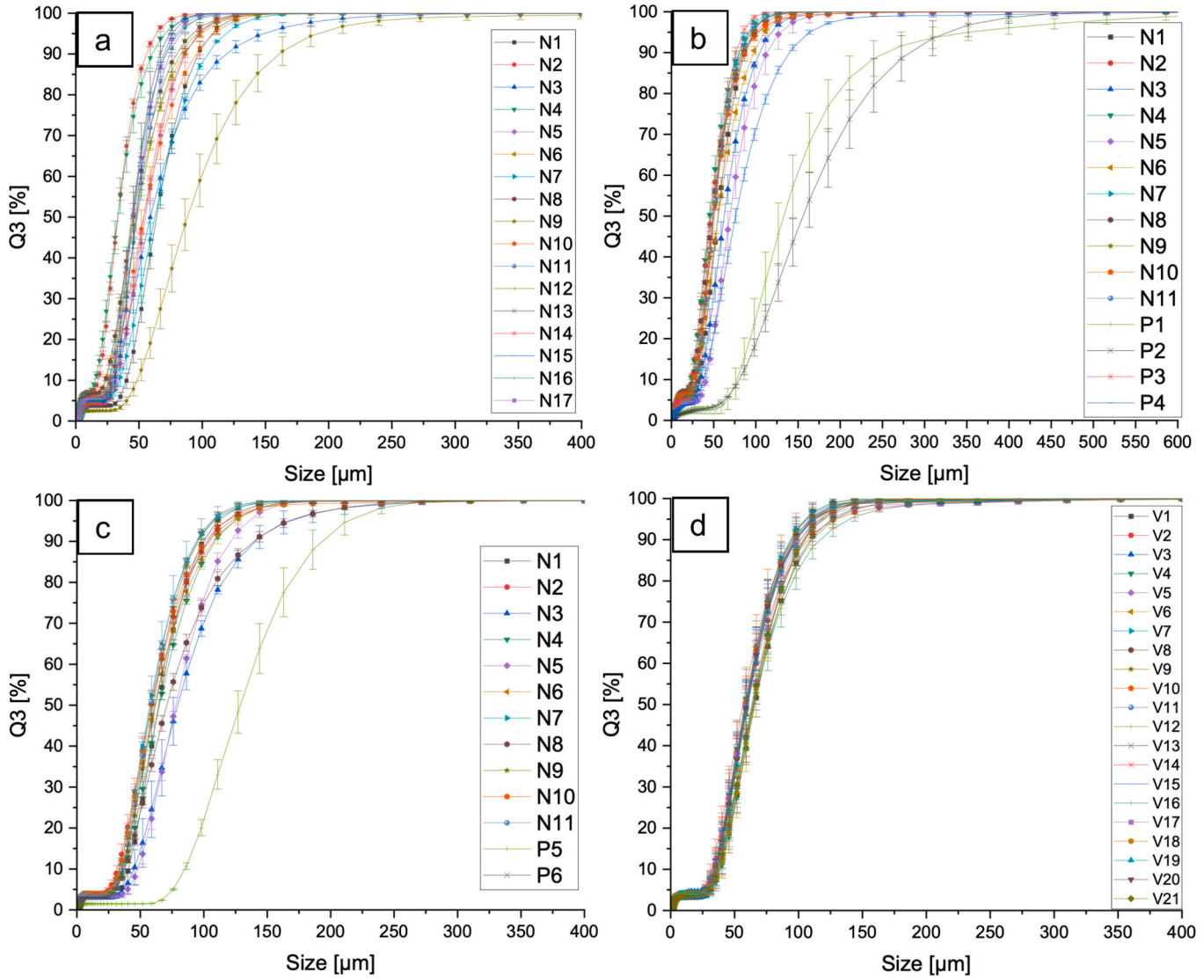

Fig. 3. Cumulativeparticle size distribution (PSD) of fabricated batches: a) PSD of GM type B batches of DoE-1; b) PSD of preliminary GM type B batches and GM type B batches of DoE-2; c) PSD of preliminary GM type A batches and GM type A batches of DoE-3; d) verification batches of GM (GM type B) that were fabricated using the same factor settings, SS: 700 rpm, T: 50 °C, R: 0.125. Results were expressed as volume distribution (mean ± standard deviation, n = 3 (technical replicates)).

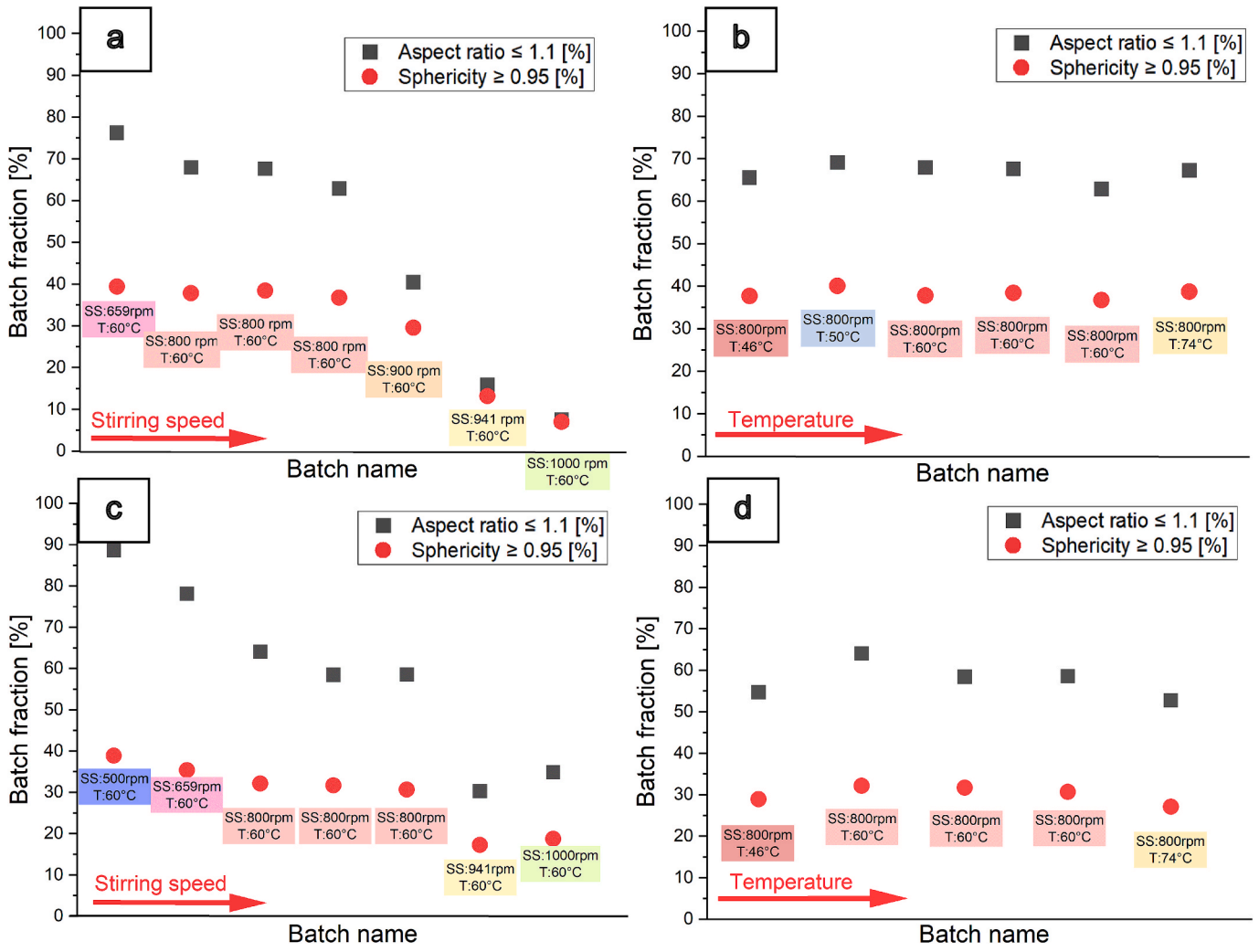

Fig. 4. Effects of process parameters stirring speed (SS) and temperature (T) on GM batch fractions with AR ≤ 1.1 or SPH ≥ 0.95. GM type B: (a) effect of SS at constant T of 60 °C, b) effect of T at constant SS of 800 rpm. GM type A: (c) effect of SS at constant T of 60 °C, and d) effect of T at constant SS of 800 rpm. Factor R was constant (0.250) for all batches. Red arrows show the direction where batch factor setting was increased. Each box color illustrates the batch factor settings.

solutions of the two gelatin types. The correlation between molecular weight distribution and Bloom number for different gelatin types was already reported in several studies (de Farias et al., 2023; Eysturskarð et al., 2009; He et al., 2024; Netter et al., 2020). For instance, Netter et al. reported a correlation between the weight-averaged molecular weight (M_w), dispersity (Đ), and Bloom number of type A gelatin samples within the investigated range of 180 g to 260 g. Their results demonstrated that gelatin samples with higher Bloom numbers exhibited higher M_w with lower Đ, and vice versa (Netter et al., 2020). Furthermore, He et al. reported a slight positive correlation between Bloom number and viscosity at 40 °C for food-grade gelatin type B solutions (He et al., 2024). SS and average particle size of both GM type A and GM type B showed an indirect correlation (Table 1 for batch codes). Moreover, using Mark-Houwink equation, de Farias et al. calculated the viscosity-average molecular weight for the same gelatin grades that we used in our study. Viscosity-average molecular weight reported in this study were 98.4 ± 1.3 kDa and 48.8 ± 2.8 kDa for gelatin type A with a Bloom number of 300 g and gelatin type B (Bloom: 225 g), respectively (de Farias et al., 2023). Since the same gelatin grades were used in our study, the formation of larger particles in GM type A under the same temperature and energy input settings may be attributed to a higher viscosity of the dispersed phase during emulsification, resulting in reduced droplet fragmentation and larger GM. Verification batches were fabricated to check the performance of the process for GM type B and high process reproducibility at constant factor settings was found (Fig. 3d).

Fig. 4 illustrates particle shape parameters of GM batches fabricated at a R of 0.250 (R = +1) at varying SS and T. The batch fraction of particles with SPH ≥ 0.95 or AR ≤ 1.1 [%] were considered as “very spherical” and “spherical”, respectively. The set of DoE aimed to maximize these fractions. For both GM types, an increase in SS was clearly associated with a reduction in the fraction of particles with SPH ≥ 0.95

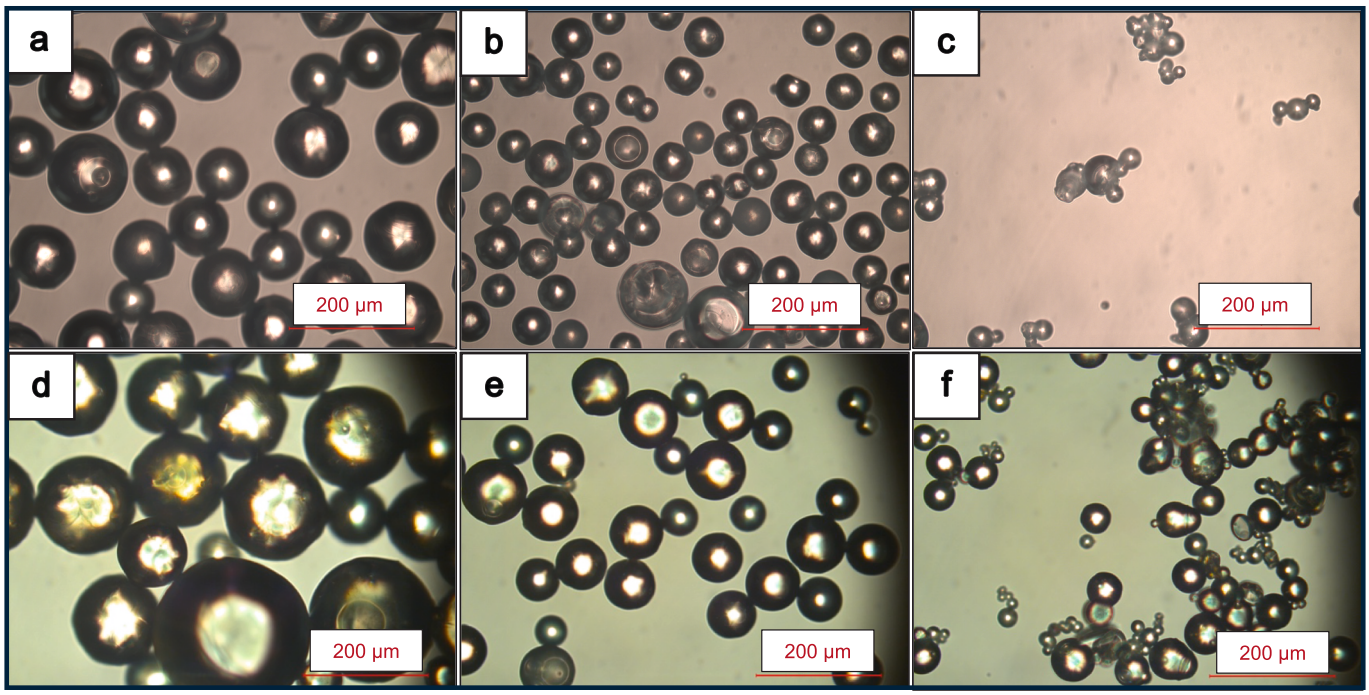

Fig. 5. Light micrograms of GM illustrating shape and size fabricated at R = 0.250. GM type B fabricated at a) SS: 500 rpm, T: 40 °C; b) SS: 659 rpm, T: 60 °C and c) SS: 1000 rpm, T: 60 °C. GM type A fabricated at d) SS: 500 rpm T: 60 °C; e) SS: 659 rpm, T: 60 °C and f) SS: 1000 rpm, T: 60 °C.

Table 2
List of model metrics and response transformations of the executed DoEs.

DoE name	Response	Response Transformation	R2	Q2	Model validity	Model reproducibility
DoE-1	D[4,3] [µm]	None	0.940	0.547	0.321	0.984
	IQR [µm]	$\log_{10}(Y+1)$	0.979	0.889	0.942	0.814
	SPH ≥ 0.95 [%]	$-\log_{10}(100-2.27*Y)$	0.968	0.773	0.954	0.979
	AR ≤ 1.1 [%]	$-\log_{10}(100-Y)$	0.965	0.729	0.953	0.962
DoE-2	D[4,3] [µm]	None	0.930	0.517	0.093	0.995
	IQR [µm]	$\log_{10}(Y)$	0.943	0.774	0.935	0.926
	SPH ≥ 0.95 [%]	$-\log_{10}(100-2*Y)$	0.994	0.988	0.733	0.960
	AR ≤ 1.1 [%]	$-\log_{10}(100-Y)$	0.989	0.978	0.077	0.997
DoE-3	D[4,3] [µm]	None	0.994	0.981	0.981	0.975
	IQR [µm]	None	0.937	0.675	0.844	0.874
	SPH ≥ 0.95 [%]	None	0.995	0.978	0.917	0.986
	AR ≤ 1.1 [%]	None	0.988	0.951	0.944	0.959

or AR ≤ 1.1 [%]. Both GM types showed a drastic reduction in such fractions at SS higher than 800 rpm. This is further illustrated by the micrographs in Fig. 5c and Fig. 5f, where batches fabricated at a SS of 1000 rpm showed extreme agglomeration and fusion, resulting in predominantly irregular particle shapes. For GM type B, the effect of temperature on particle shape was not clearly noticeable (Fig. 4b). whereas a slight negative quadratic effect of temperature on the batch fraction of spherical particles was observed for GM type A (Fig. 4d).

Model metrics of the three DoE are summarized in Table 2. DoE-3, focusing on GM type A, revealed a good data fit with high prediction power for all investigated responses. In contrast, models created on GM type B manufacturing through DoE-1 and DoE-2 exhibited relatively poor prediction power for the response D[4,3]. Although the lack-of-fit test was insignificant in DoE-2, it was statistically significant for the response D[4,3] in DoE-1 ($p = 0.027$, Supplementary Table S1), indicating that this model has limitations in providing accurate absolute predictions for D[4,3]. Nevertheless, the size trends remain noticeable in both DoE-1 and DoE-2 through coefficients plots. ANOVA table and observed versus predicted plots for each DoE can be found in the in Supplementary figure S2.

Coefficient plots for three-factor DoE (DoE-1) and two-factor DoE (DoE-2) for GM type B were given in Fig. 6. Both DoEs reveal that SS had the largest significant effect on GM size. The first order effect of SS was negative, indicating that mean particle diameter (D[4,3]) decreased with increasing SS. In addition, a positive quadratic effect of SS most probably indicates that at high SS a deviation from the linear trend was significant and that after a minimum averaged particle size, the values increased again at high SS. In general, it was known in emulsion production processes as well that finer droplets exhibit higher Laplace pressure and there is a need for even higher energy input to fragment such droplets (Yadav and Kale, 2019). Therefore, the relationship between energy input and droplet fragmentation is not expected to follow a linear trend, even in kinetically stabilized emulsions. A similar behavior is considered responsible for the trends observed in our GM fabrication process. Coefficient plots for particle shape responses exhibited correlations consistent with the observed size pattern. The batch fraction of spherical particles (SPH ≥ 0.95 or AR ≤ 1.1) [%] decreased in both linear and quadratic trends with increasing SS, indicating a higher fraction of agglomerated and fused particles upon high process energy input. At high SS, the fabrication process initially produces an emulsion with finer droplets, which theoretically exhibit higher Gibbs free energy (Gonzalez Ortiz et al., 2020) compared to

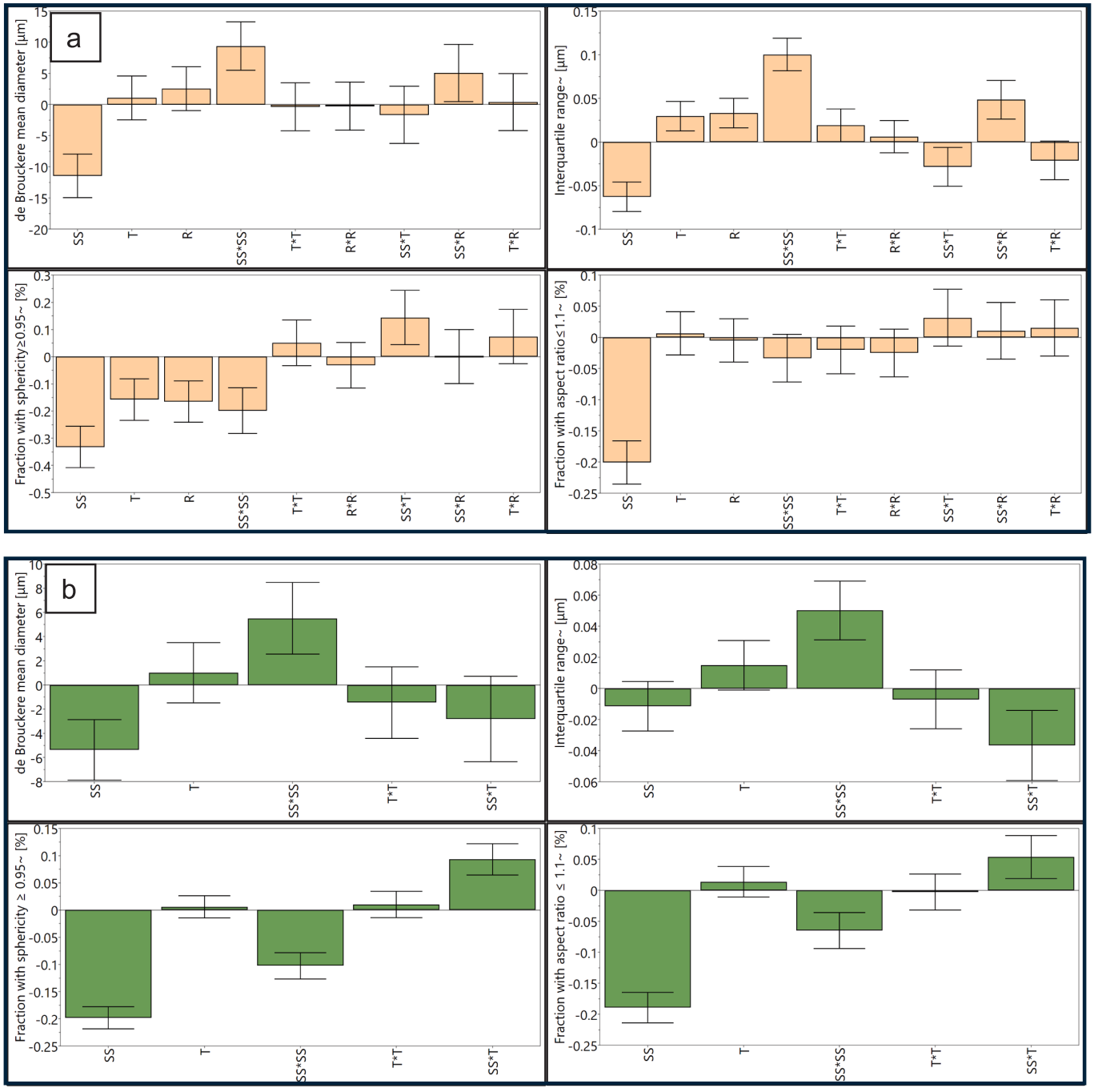

Fig. 6. Scaled and centered coefficients plots of the full quadratic model of GM type B. a) Coefficients plot of DoE-1: β0 coefficients are as follows: de Brouckere mean diameter [µm]: 47.41 ± 7.47, Interquartile range [µm]: 1.36 ± 0.04, Fraction with SPH ≥ 0.95 [%]: −0.86 ± 0.16, Fraction with AR ≤ 1.1 [%]: −1.49 ± 0.07; b) Coefficients plot of DoE-2, β0 coefficients are as follows: de Brouckere mean diameter: 53.16 ± 4.08, Interquartile range: 1.45 ± 0.03, Fraction with SPH ≥ 0.95: −1.39 ± 0.03, Fraction with AR ≤ 1.1: −1.53 ± 0.04. Coefficients for certain responses (see Table 2) were calculated using transformed responses and were expressed as mean ± confidence intervals (confidence level: 95 %).

coarser droplets, resulting a state with lower thermodynamic stability. Since our fabrication strategy did not include additional kinetic stabilizers such as emulsifiers, this unstable state is more susceptible to either emulsion instabilities, such as flocculation and coalescence during emulsification, or agglomeration during the thermal gelation stage. In the thermal gelation stage, fine (either flocculated or separate) droplets were assumed to form particle agglomerates. The formation of fused particles observed in Fig. 5c and f is likely a result of a fusion of agglomerated particles during the stage of particle hardening by water extraction using acetone. Moreover, a similar trend was observed in

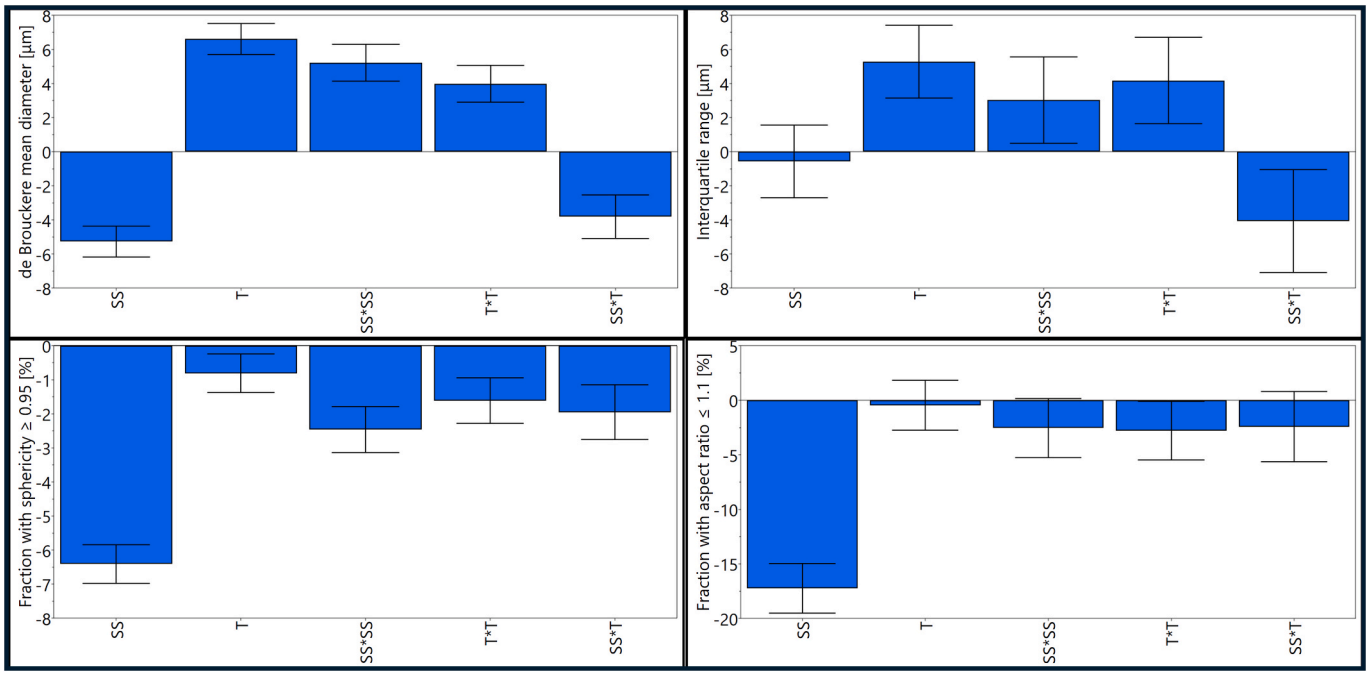

Fig. 7. Scaled and centered coefficients plots of the full quadratic model of GM type A fabrication (DoE-3). β0 coefficients are as follows: de Brouckere mean diameter [µm]: 62.59 ± 1.48; Interquartile range [µm]: 31.59 ± 3.49; Fraction with SPH ≥ 0.95 [%]: 31.49 ± 0.92 and Fraction with AR ≤ 1.1 [%]: 60.36 ± 3.71. Coefficients were expressed as mean ± confidence intervals (confidence level: 95 %).

micrographs of freshly isolated GM dispersed in acetone without drying (Supplementary figure S3), further supporting the assumption that particle agglomeration and fusion occurred during the fabrication process. Positive quadratic effect of SS on IQR of the batch particle size distribution also suggested that lower thermodynamic stability at high SS might have induced droplet coalescence and increased the interquartile range of the batch particle size distribution.

The effect of process temperature (T) on particle size and shape responses in GM type B fabrication appeared to be less straightforward than that of SS in both DoE-1 and DoE-2. Higher process temperatures were anticipated to lower the viscosity of both dispersed and continuous phases of the initially formed emulsion, which in turn would be expected to promote greater droplet fragmentation. On the other hand, high temperatures were also presumed to result in a state of lower thermodynamic stability, which is likely to promote instabilities. For GM type B, both DoE-1 and DoE-2 suggested that temperature affected all responses primarily through interaction effects (Fig. 6). For GM type A, on the other hand, a direct effect of temperature on fabrication process was identified (Fig. 7). Temperature exhibited a positive correlation with D[4,3] through both linear and quadratic effects. Additionally, process temperature had significant negative linear and quadratic effects on the batch fraction of particles with SPH ≥ 0.95, as well as a significant negative quadratic effect on the fraction of particles with an AR ≤ 1.1. Therefore, the observed increase in batch D[4,3] at elevated process temperatures appears to be attributed to an increased tendency for particle agglomeration within the batches for GM type A. The main effect of temperature on the interquartile range (IQR) of the batch particle size distribution (PSD) was significant across DoE-1 and DoE-3, which may indicate the occurrence of droplet coalescence at elevated temperatures.

An effect of volume ratio of dispersed phase to continuous phase for kinetically stabilized emulsions on droplet dimensions was proposed by Davies and Godfrey et. al. through the following equation (Eq. (3)) (Davies, 1992; Godfrey et al., 1989).

$$\frac{D[3,2]}{D} = k_1(1 + k_2\phi_d)We^{-0.6} \quad (3)$$

where, D[3,2] is a Sauter mean diameter of an emulsion droplet size distribution, D is a stirrer diameter, k_1 and k_2 are coefficients, ϕ_d is the volume ratio of dispersed phase-to-continuous phase (R), and We is a Weber number. The droplet Sauter mean diameter was proposed to increase by higher ϕ_d. It was later suggested that higher R is likely to increase the frequency of droplet collisions, thereby promoting coalescence events and ultimately leading to an increase in the mean droplet size (Heiskanen et al., 2012; Leng and Calabrese, 2003). Furthermore, Peng et al. reported a reduction in particle size at low R when GM were fabricated via W/O emulsion method, using sorbitan monooleate as an emulsifying agent (Peng et al., 2011). We investigated the impact of R on GM type B fabrication process in a three-factor DoE (DoE-1) (Fig. 6). Coefficients plots showed a slight increase in batch mean diameter D[4,3] once GM was fabricated with high R, although the main effect of R was not significant. The impact of R can however be seen though a significant interaction effect with SS (SS*R), implying a positive correlation with D[4,3]. The positive significant main effect of R on the response IQR on the other hand could indicate an increased number of droplet coalescence events at high dispersed phase volumes

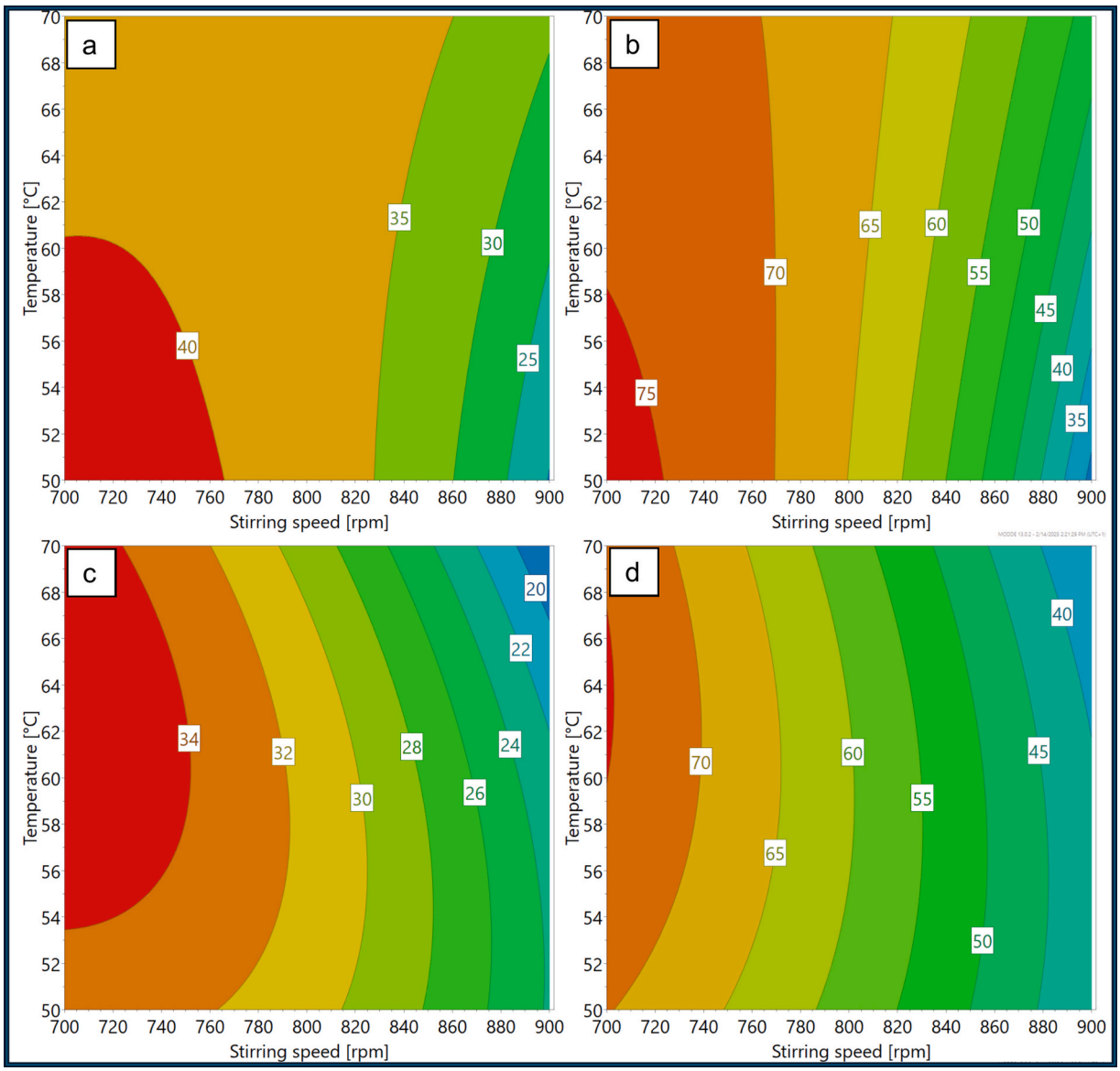

Fig. 8. Response contour plots for shape responses for GM type B (DoE-1) and GM type A (DoE-3). a) Fraction with SPH $\geq$ 0.95 [%] (GM type B); b) fraction with AR $\leq$ 1.1 [%] (GM type B); c) fraction with SPH $\geq$ 0.95 [%] (GM type A) and d) fraction with SPH $\geq$ 0.95 [%] (GM type A).

during the emulsion stage of our GM fabrication process – a phenomenon that aligns with suggestions proposed for stabilized emulsions (Heiskanen et al., 2012; Leng and Calabrese, 2003). Particle shape was also influenced by R. The main effect of R on the batch fraction of particles with SPH $\geq$ 0.95 revealed a significant negative correlation, suggesting that higher dispersed phase volumes contribute to increased shape irregularities in the final particles.

Fig. 8 presents the response contour plots from the two-factor DoEs for GM type A and type B, illustrating the effects of factors SS and T on particle shape parameters. Both models illustrate that low stirring speeds increased particle sphericity. For GM type B, process temperatures below 58 °C combined with stirring speeds lower than 720 rpm were found to produce microparticles with the highest batch fraction of particles exhibiting AR $\leq$ 1.1. Concomitantly, these conditions are associated with an increase in particle size. The similar trends were also noticeable in GM type A except slightly higher temperatures in a combination with low stirring speeds would yield the highest batch fraction of particles with SPH $\geq$ 0.95 or/and AR $\leq$ 1.1.

The sweet spot plot of particle size and shape responses for GM type A (DoE-3) (Fig. 9) illustrates that maximization of batch fraction of SPH $\geq$ 0.95 and AR $\leq$ 1.1 during fabrication requires a compromise with particle size. Specifically, factor settings that produce a slightly larger mean particle size (D[4,3]) promote a higher batch fraction of particles with good shape quality (SPH $\geq$ 0.95 and/or AR $\leq$ 1.1).

4. Conclusion

The present study systematically investigated the fabrication of microparticles from gelatin type A and type B via a water-in-oil (W/O) emulsion method, employing design of experiments statistics. Effects of process stirring speed, temperature, phase volume ratio (R) on particle size distribution and two specific shape parameters were investigated. Particle size reduction at high stirring speeds reduced particle shape parameter SPH and AR, indicating a high agglomeration tendency fine GM derived from both gelatin types. R exhibited a negative main effect on fraction yield with SPH $\geq$ 0.95 in GM type B indicating increasing deviation form a spherical particle shape when particle fabrication was attempted with large gelatin solution volumes. The process temperature affected fabrication of GM type A more than GM type B. Overall, the models derived from the experimental sets showed that particle size

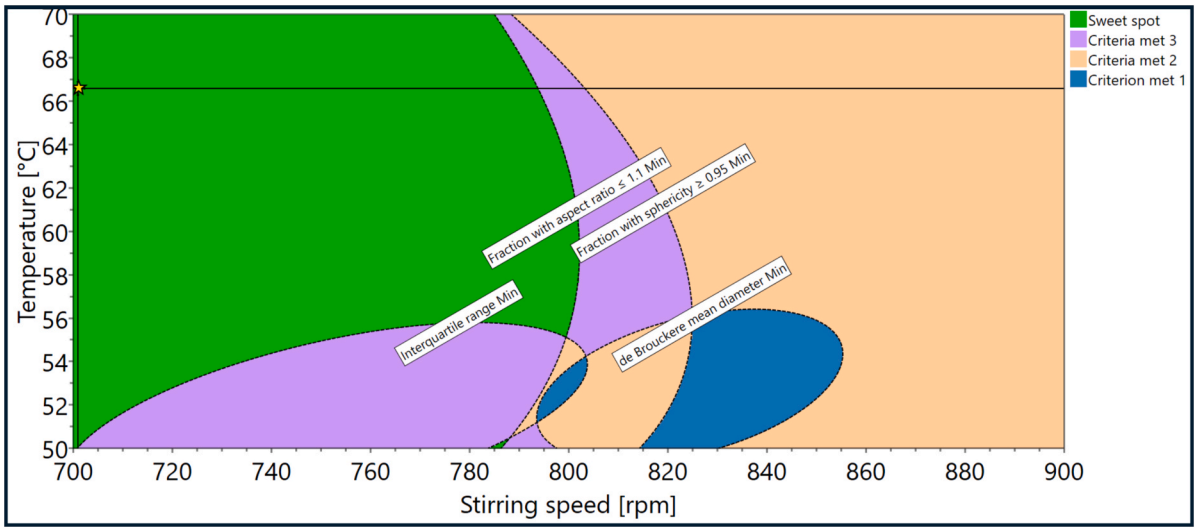

Fig. 9. The sweet spot plot generated for GM type A (DoE-3) highlights the robust set-point with a star symbol. To generate the plot, following response ranges (criteria) were selected: de Brouckere mean diameter (60–100 μm), Interquartile range (30–60 μm), fraction with SPH ≥ 0.95 (30–45 %), and fraction with AR ≤ 1.1 (60–90 %). The objective was to maximize SPH ≥ 0.95 and AR ≤ 1.1 while maintaining the particle size responses within the range of 60–100 μm. The zone in which 1 criterion is met is colored blue. The zones in which 2 and 3 parameters are reached a colored tan and lavender, respectively. The sweet spot area (all four criteria met) is represented in green. Robust set-point (shown with yellow star and coordinated with black lines) was predicted to generate particles with D[4,3]: 82 μm, IQR: 43 μm, SPH ≥ 0.95: 35.46 % and AR ≤ 1.1: 75.00 % with the probabilities of failure of 0 %, 0.33 %, 0.10 % and 0.46 %, respectively.

distribution and shape quality of GM, for both gelatin types, can be effectively controlled by modifying the factor settings. Optimized shape parameters, which are considered critical for particle quality after further crosslinking of the particles, required fabrication with a lower stirring speeds and lower R as previously published (Hinkelmann et al., 2022a; Hinkelmann et al., 2022b; Loth et al., 2014). To our knowledge, this is the first study to investigate the W/O emulsion-based fabrication of pristine gelatin microparticles using DoE statistics, considering both particle size distribution and shape parameters. Therefore, this work is anticipated to provide a solid starting point for future studies, aiming to control particle size and shape prior to particle crosslinking.

CRediT authorship contribution statement

Burak Demir: Writing – review & editing, Writing – original draft, Methodology, Investigation, Conceptualization. **Michael C. Hacker:** Writing – review & editing, Supervision, Funding acquisition, Formal analysis, Conceptualization.

Declaration of competing interest

The authors declare that they have no known competing financial interests or personal relationships that could have appeared to influence the work reported in this paper.

Appendix A. Supplementary material

Supplementary data to this article can be found online at https://doi.org/10.1016/j.ijpharm.2025.126302.

Data availability

Data will be made available on request.

References

Annamalai, R.T., Turner, P.A., Carson, W.F., Levi, B., Kunkel, S., Stegemann, J.P., 2018. Harnessing macrophage-mediated degradation of gelatin microspheres for spatiotemporal control of BMP2 release. Biomaterials 161, 216–227.

Behrend-Keim, B., Castro-Munoz, A., Monrreal-Ortega, L., Avalos-Leon, B., Campos-Estrada, C., Smyth, H.D.C., Bahamondez-Canas, T.F., Moraga-Espinoza, D., 2023. The forgotten material: highly dispersible and swellable gelatin-based microspheres for pulmonary drug delivery of cromolyn sodium and ipratropium bromide. Int. J. Pharm. 644, 123331.

Bruschi, M.L., Cardoso, M.L., Lucchesi, M.B., Gremiao, M.P., 2003. Gelatin microparticles containing propolis obtained by spray-drying technique: preparation and characterization. Int. J. Pharm. 264, 45–55.

Cao, S., Li, L., Du, Y., Gan, J., Wang, J., Wang, T., Liu, Y., Liu, W., Zhou, Y., Gao, X., Li, H., Liu, T., 2021. Porous gelatin microspheres for controlled drug delivery with high hemostatic efficacy. Colloids Surf. B Biointerfaces 207, 112013.

Choy, Y.B., Cheng, F., Choi, H., Kim, K., 2008. Monodisperse gelatin microspheres as a drug delivery vehicle: release profile and effect of crosslinking density. Macromol. Biosci. 8, 758–765.

Curcio, M., Gianfranco Spizzirri, U., Iemma, F., Puoci, F., Cirillo, G., Parisi, O.I., Picci, N., 2010. Grafted thermo-responsive gelatin microspheres as delivery systems in triggered drug release. Eur. J. Pharm. Biopharm. 76, 48–55.

D'Angelo, F., Tiribuzi, R., Armentano, I., Kenny, J.M., Martino, S., Orlacchio, A., 2011. Mechanotransduction: tuning stem cells fate. J. Funct. Biomater. 2, 67–87.

Davies, G., 1992. Mixing and coalescence phenomena in liquid–liquid systems. In: Science and Practice of Liquid-Liquid Extraction. Clarendon Press, Oxford/UK, pp. 244–342.

de Farias, B.S., Rizzi, F.Z., Ribeiro, E.S., Diaz, P.S., Sant'Anna Cadaval, T.R., Dotto, G.L., Khan, M.R., Manoharadas, S., de Almeida Pinto, L.A., Dos Reis, G.S., 2023. Influence of gelatin type on physicochemical properties of electrospun nanofibers. Sci. Rep. 13, 15195.

Eysturskarð, J., Haug, I.J., Ulset, A.-S., Draget, K.I., 2009. Mechanical properties of mammalian and fish gelatins based on their weight average molecular weight and molecular weight distribution. Food Hydrocoll. 23, 2315–2321.

Foox, M., Zilberman, M., 2015. Drug delivery from gelatin-based systems. Expert Opin. Drug Deliv. 12, 1547–1563.

Godfrey, J., Obi, F.N., Reeve, R., 1989. Measuring drop size in continuous liquid-liquid mixers. Chem. Eng. Prog. 85, 61–69.

Gonzalez Ortiz, D., Pochat-Bohatier, C., Cambedouzou, J., Bechelany, M., Miele, P., 2020. Current trends in pickering emulsions: particle morphology and applications. Engineering 6, 468–482.

Gunji, S., Obama, K., Matsui, M., Tabata, Y., Sakai, Y., 2013. A novel drug delivery system of intraperitoneal chemotherapy for peritoneal carcinomatosis using gelatin microspheres incorporating cisplatin. Surgery 154, 991–999.

He, C., Ma, D., Zeng, M., Wang, Z., Chen, Q., Chen, J., He, Z., 2024. Effect of molecular weight distributions on the gelation rate and other physicochemical properties of bovine bone gelatin (Type B). Food Biosci. 57.

Heiskanen, H., Denifl, P., Pitkänen, P., Hurme, M., 2012. Effect of preparation conditions on the properties of microspheres prepared using an emulsion-solvent extraction process. Chem. Eng. Res. Des. 90, 1517–1526.

Hinkelmann, S., Springwald, A.H., Schulze, S., Hempel, U., Mitrach, F., Wolk, C., Hacker, M.C., Schulz-Siegmund, M., 2022a. Mineralizing gelatin microparticles as cell carrier and drug delivery system for siRNA for bone tissue engineering. Pharmaceutics 14.

Hinkelmann, S., Springwald, A.H., Starke, A., Kalwa, H., Wolk, C., Hacker, M.C., Schulz-Siegmund, M., 2022b. Microtissues from mesenchymal stem cells and siRNA-loaded

cross-linked gelatin microparticles for bone regeneration. Mater. Today Bio 13, 100190.
Jung, J., Oh, J., 2014. Swelling characterization of photo-cross-linked gelatin methacrylate spherical microgels for bioencapsulation. e-Polymers 14, 161–168.
Kleinebudde, P., 1995. Use of a power-consumption-controlled extruder in the development of pellet formulations. J. Pharm. Sci. 84, 1259–1264.
Kong, Y.-Q., Li, D., Wang, L.-J., Adhikari, B., 2011. Preparation of gelatin microparticles using water-in-water (w/w) emulsification technique. J. Food Eng. 103, 9–13.
Leng, D.E., Calabrese, R.V., 2003. Immiscible liquid–liquid systems. In: Handbook of Industrial Mixing: Science and Practice. John Wiley & Sons Inc., NJ, pp. 639–753.
Loth, T., Hotzel, R., Kascholke, C., Anderegg, U., Schulz-Siegmund, M., Hacker, M.C., 2014. Gelatin-based biomaterial engineering with anhydride-containing oligomeric cross-linkers. Biomacromolecules 15, 2104–2118.
Lu, S., Lee, E.J., Lam, J., Tabata, Y., Mikos, A.G., 2016. Evaluation of gelatin microparticles as adherent-substrates for mesenchymal stem cells in a hydrogel composite. Ann. Biomed. Eng. 44, 1894–1907.
Netter, A.B., Goudoulas, T.B., Germann, N., 2020. Effects of Bloom number on phase transition of gelatin determined by means of rheological characterization. LWT-Food Sci. Technol. 132.
Nguyen, A.H., McKinney, J., Miller, T., Bongiorno, T., McDevitt, T.C., 2015. Gelatin methacrylate microspheres for controlled growth factor release. Acta Biomater. 13, 101–110.
Nii, T., 2021. Strategies using gelatin microparticles for regenerative therapy and drug screening applications. Molecules 26.
Nouri-Felekori, M., Khakbiz, M., Nezafati, N., Mohammadi, J., Eslaminejad, M.B., 2019. Comparative analysis and properties evaluation of gelatin microspheres crosslinked with glutaraldehyde and 3-glycidoxypropyltrimethoxysilane as drug delivery systems for the antibiotic vancomycin. Int. J. Pharm. 557, 208–220.
Obata, Y., Nishino, T., Kushibiki, T., Tomoshige, R., Xia, Z., Miyazaki, M., Abe, K., Koji, T., Tabata, Y., Kohno, S., 2012. HSP47 siRNA conjugated with cationized gelatin microspheres suppresses peritoneal fibrosis in mice. Acta Biomater. 8, 2688–2696.
Park, K.-S., Kim, C., Nam, J.-O., Kang, S.-M., Lee, C.-S., 2016. Synthesis and characterization of thermosensitive gelatin hydrogel microspheres in a microfluidic system. Macromol. Res. 24, 529–536.
Patel, Z.S., Yamamoto, M., Ueda, H., Tabata, Y., Mikos, A.G., 2008. Biodegradable gelatin microparticles as delivery systems for the controlled release of bone morphogenetic protein-2. Acta Biomater. 4, 1126–1138.
Pearce, H.A., Kim, Y.S., Watson, E., Bahrami, K., Smoak, M.M., Jiang, E.Y., Elder, M., Shannon, T., Mikos, A.G., 2021. Development of a modular, biocompatible thiolated gelatin microparticle platform for drug delivery and tissue engineering applications. Regen Biomater 8, rbab012.
Peng, Z.Y., Shen, Y.Q., Li, Z.P., 2011. Control of size and morphology of gelatin microspheres. J. Macromol. Sci. Part B 51, 12–21.
Sakai, S., Ito, S., Inagaki, H., Hirose, K., Matsuyama, T., Taya, M., Kawakami, K., 2011. Cell-enclosing gelatin-based microcapsule production for tissue engineering using a microfluidic flow-focusing system. Biomicrofluidics 5, 13402.
Standardization, I.O.f., 2008. ISO 9276–6: Representation of results of particle size analysis — Part 6: Descriptive and quantitative representation of particle shape and morphology. ISO, Geneva, Switzerland.
Tran, T.H., Ramasamy, T., Poudel, B.K., Marasini, N., Moon, B.K., Cho, H.J., Choi, H.-G., Yong, C.S., Kim, J.O., 2013. Preparation and characterization of spray-dried gelatin microspheres encapsulating ganciclovir. Macromol. Res. 22, 124–130.
Turner, P.A., Thiele, J.S., Stegemann, J.P., 2017. Growth factor sequestration and enzyme-mediated release from genipin-crosslinked gelatin microspheres. J. Biomater. Sci. Polym. Ed. 28, 1826–1846.
Vandelli, M.A., Rivasi, F., Guerra, P., Forni, F., Arletti, R., 2001. Gelatin microspheres crosslinked with d,l-glyceraldehyde as a potential drug delivery system: preparation, characterisation, in vitro and in vivo studies. Int. J. Pharm. 215, 175–184.
Wang, J., Tauchi, Y., Deguchi, Y., Morimoto, K., Tabata, Y., Ikada, Y., 2000. Positively charged gelatin microspheres as gastric mucoadhesive drug delivery system for eradication of H. pylori. Drug Deliv. 7, 237–243.
Yadav, K.S., Kale, K., 2019. High pressure homogenizer in pharmaceuticals: understanding its critical processing parameters and applications. J. Pharm. Innov. 15, 690–701.
Yan, J., Miao, Y., Tan, H., Zhou, T., Ling, Z., Chen, Y., Xing, X., Hu, X., 2016. Injectable alginate/hydroxyapatite gel scaffold combined with gelatin microspheres for drug delivery and bone tissue engineering. Mater. Sci. Eng. C Mater. Biol. Appl. 63, 274–284.
Yang, J., Zhou, M., Li, W., Lin, F., Shan, G., 2020. Preparation and evaluation of sustained release platelet-rich plasma-loaded gelatin microspheres using an emulsion method. ACS Omega 5, 27113–27118.
Yeh, C.-H., Chen, K.-R., Lin, Y.-C., 2013. Developing heatable microfluidic chip to generate gelatin emulsions and microcapsules. Microfluid. Nanofluid. 15, 775–784.
Yue, J., Liu, Z., Wang, L., Wang, M., Pan, G., 2025. Recent advances in bioactive hydrogel microspheres: Material engineering strategies and biomedical prospects. Mater. Today Bio 31, 101614.